Received: 26 June 2022Accepted: 8 July 2023

DOI: 10.1111/2041-210X.14193

Methods in Ecology and Evolution

RESEARCH ARTICLE

# An integrative modelling framework for passive acoustic telemetry

Edward Lavender[1,2] | Stanisław Biber[3] | Janine Illian[4] | Mark James[2] | Peter J. Wright[5] | James Thorburn[2,6,7] | Sophie Smout[1,2]

[1]Centre for Research into Ecological and Environmental Modelling, University of St Andrews, St Andrews, UK; [2]Scottish Oceans Institute, University of St Andrews, St Andrews, UK; [3]Department of Engineering Mathematics, University of Bristol, Bristol, UK; [4]School of Mathematics and Statistics, University of Glasgow, Glasgow, UK; [5]Marine Scotland Science, Aberdeen, UK; [6]School of Applied Sciences, Edinburgh Napier University, Edinburgh, UK and [7]Centre for Conservation and Restoration Science, Edinburgh Napier University, Edinburgh, UK

**Correspondence**
Edward Lavender
Email: el72@st-andrews.ac.uk

**Funding information**
Centre for Research into Ecological and Environmental Modelling; Marine Alliance for Science and Technology for Scotland; Marine Scotland Science, Grant/Award Number: SP004 and SP02B0; NatureScot, Grant/Award Number: 015960; Shark Guardian; Scottish Funding Council

**Handling Editor:** Luca Börger

## Abstract

1. Passive acoustic telemetry is widely used to study the movements of aquatic animals. However, a holistic, mechanistic modelling framework that permits the reconstruction of fine-scale movements and emergent patterns of space use from detections at receivers remains lacking.
2. Here, we introduce an integrative modelling framework that recapitulates the movement and detection processes that generate detections to reconstruct fine-scale movements and patterns of space use. This framework is supported by a new family of algorithms designed for detection and depth observations and can be flexibly extended to incorporate other data types. Using simulation, we illustrate applications of our framework and evaluate algorithm utility and sensitivity in different settings. As a case study, we analyse movement data collected from the Critically Endangered flapper skate (*Dipturus intermedius*) in Scotland.
3. We show that our methods can be used to reconstruct fine-scale movement paths, patterns of space use and support habitat preference analyses. For reconstructing patterns of space use, simulations show that the methods are consistently more instructive than the most widely used alternative approach (the mean-position algorithm), particularly in clustered receiver arrays. For flapper skate, the reconstruction of movements reveals responses to disturbance, fine-scale spatial partitioning and patterns of space use with significant implications for marine management.
4. We conclude that this framework represents a widely applicable methodological advance with applications to studies of pelagic, demersal and benthic species across multiple spatiotemporal scales.

Sophie Smout and James Thorburn are joint senior authors.

**KEYWORDS**
biologging, biotelemetry, centre of activity, particle filtering, utilisation distribution

## 1 | INTRODUCTION

Animal movement has a pivotal influence on ecosystem structure and function (Nathan et al., 2022; Riotte-Lambert & Matthiopoulos, 2020). Within selected areas, movement can reflect habitat preferences (Mercker et al., 2021), species' interactions, such as foraging (Sims et al., 2008), and responses to disturbance (Doherty et al., 2021). Across species' distributions, movement shapes migration (Fudickar et al., 2021), redistribution (Pecl et al., 2017) and patterns of space use, with profound conservation implications (Hays et al., 2019).

Advances in biotelemetry have revealed movement trajectories in unprecedented detail (Nathan et al., 2022). In aquatic environments, satellite tracking has been widely exploited but is limited by the time individuals spend at the surface (Hussey et al., 2015). However, over large spatial scales (typically, hundreds of kilometres), global location sensors have been coupled with latent-variable modelling to reconstruct the movements of pelagic and demersal species (Block et al., 2005; Pedersen et al., 2008). Meanwhile, at fine spatial scales (typically, hundreds of metres), acoustic positioning systems have been used to reconstruct movements via multilateration (Orrell & Hussey, 2022). Passive acoustic telemetry (PAT) fills a gap between these systems (Matley et al., 2022). PAT generally comprises a static array of receivers with nonoverlapping detection ranges that record individual-specific detections of tagged animals within range. Yet while detections can indicate broad-scale features of movement, such as occupancy, gaps in detections challenge the reconstruction of movements and patterns of space use.

Four main approaches have been developed to reconstruct movements or patterns of space use from detections. The first simply maps detections (Lavender et al., 2021a). The second (and most common) approach estimates 'centres of activity' (COAs), usually as weighted averages of the locations at which detections were recorded over consecutive time intervals (the mean-position algorithm) (Simpfendorfer et al., 2002). COAs are translated into maps of space use via smoothing techniques such as kernel utilisation distribution (KUD) estimation (Udyawer et al., 2018). Network analysis is a third approach which treats receivers as nodes on a network that are connected by edges defined by sequential detections (Lea et al., 2016). However, these approaches do not represent the processes that generate observations, including movement and the detection process. Consequently, the movements that generate observations remain unresolved and maps of space use may be substantially influenced by array design. Building on this limitation, latent-variable models represent a fourth approach (Hostetter & Royle, 2020; Pedersen & Weng, 2013; Winton et al., 2018). These models treat individual locations as latent variables that are linked, via movement and observation models, to detections. Yet existing latent-variable models for PAT cannot easily incorporate ancillary information on location, such as depth observations, that is often collected alongside detections. The incorporation of movement barriers, such as coastline, also currently requires bespoke Bayesian model-fitting algorithms that are computationally intensive.

A fifth 'synthetic path' class of approaches has been developed with the potential to address these shortcomings. These approaches generate movement path(s) that are consistent with the observations. In the 'refined-shortest paths' implementation, one path (the shortest) is generated between the receivers that recorded sequential detections and used to fit a dynamic Brownian bridge movement model that incorporates uncertainty with movement away from receivers (Niella et al., 2020). Aspillaga et al.'s (2019) related simulation-based method generates multiple least-cost paths to map space use. Yet while this method offers promise for capturing the movement and detection processes that generate observations, a holistic, mechanistic modelling framework for achieving this goal remains lacking.

This study establishes a comprehensive, stochastic, 'synthetic path' modelling framework for detections that can incorporate observations, the detection process and properties of movement to reconstruct fine-scale movement paths and emergent patterns of space use. Key innovations include the exploitation of detection gaps alongside detections, the incorporation of multiple datasets and the comprehensive recapitulation of the movement and detection processes that generate observations. These advances permit the reconstruction of movement paths and refined maps of space use, informing analyses of fine-scale movements, residency and habitat preferences. The framework splits the inference process into two stages. In the first stage, each source of observations is used to establish the set of locations in which a tagged individual could have been located through time. We introduce the 'acoustic-container' (AC) branch of algorithms for capturing the information provided by detection and depth observations in this stage, but other data types could be combined in the same way. In the second stage, a particle filtering (PF) process is used to incorporate movement. Alongside the central framework, the coupling of the AC-branch and PF-branch algorithms collectively represents a new family of algorithms for inferring movements and patterns of space use termed the 'flapper family', following its motivation by research on the Critically Endangered flapper skate (*Dipturus intermedius*) (Dodd et al., 2022; Lavender et al., 2021a, 2021b; Lavender, Aleynik, Dodd, Illian, James, Smout, et al., 2022; Lavender, Aleynik, Dodd, Illian, James, Wright, et al., 2022; Thorburn et al., 2021). To support algorithm application, we introduce the flapper R package. Using simulation, we illustrate algorithm applications and examine their utility and sensitivity in different settings. Using flapper skate data, we demonstrate real-world applications for reconstructing fine-scale movements, refined maps of space use and in habitat preference analyses.

## 2 | MATERIALS AND METHODS

### 2.1 | Conceptual overview

The framework advanced here recognises two sources of information on movement trajectories in PAT systems. Information on location is the first: at any one time, detections (or lack thereof), alongside other observations, restrict our uncertainty in an animal's possible location. Information on movement is the second: at any one time, given a previous location, movement limitations restrict our uncertainty in possible future locations. This distinction translates into a two-stage modelling framework. The first stage reconstructs the set of locations in which a tagged individual could have been located through time, given available data, using an AC-branch algorithm. The second stage uses movement restrictions to connect sequential locations, using a PF-branch algorithm.

We introduce three AC-branch algorithms and three corresponding PF-branch algorithms. The first-stage AC algorithm is the backbone of the framework, capturing the information provided by PAT to define the set of possible locations of an individual through time. In an extension for depth observations, we introduce the depth-contour (DC) algorithm and show how the AC and DC algorithms can be combined via the ACDC algorithm. For each AC-branch algorithm, we identify its corresponding PF-branch counterpart (the ACPF, DCPF and ACDCPF algorithms). Collectively, these are termed the 'flapper algorithms' (Table 1). Here, we consider these algorithms in discretised form with locations represented on a uniform grid and denote the coordinates of cell $i$'s midpoint by $\boldsymbol{s}^i$. For graphical descriptions, see Figures S1–S5.

### 2.2 | Acoustic-container algorithm

The AC algorithm is designed to capture the information provided by detections (Figure S1). The crux is that detections anchor our knowledge of an individual's location around receivers, while in the gaps between detections the area within which an individual could be located expands beyond the receiver that recorded the previous detection while shrinking towards the receiver that recorded the next detection, in line with the individual's movement capabilities. The dynamics of this process are captured by the expansion, contraction and intersection of areas termed 'acoustic containers' that define the set of possible locations of an individual according to receiver(s). We describe these dynamics for a simple array with non-overlapping receivers here and generalise the description in the Supporting Information S1.1.

**TABLE 1** The flapper algorithms. The family comprises three AC-branch algorithms and three corresponding PF-branch algorithms. Together, the AC and ACPF algorithms provide a framework for the stochastic modelling of PAT data and the DC, DCPF, ACDC and ACDCPF algorithms represent modifications/extensions of this framework that incorporate depth observations.

| AC branch | PF branch |
|---|---|
| AC | ACPF |
| DC | DCPF |
| ACDC | ACDCPF |

Let us consider a sequence of time steps, indexed by $t$, along which detections of a tagged individual, indexed by $t_{acc}$, are recorded at regular or irregular intervals (Figure S1). For each pair of detections, we can consider the individual's location from ($A$) the perspective of the receiver at which it was just detected (or its previous location) and ($B$) the receiver at which it was next detected. At the moment of the first detection ($t = 1$ and $t_{acc} = 1$), from perspective $A$, the individual must be within the receiver's maximum detection range ($\gamma$), excluding any inhospitable habitats ($U$), in an area termed the 'detection container'. If we denote a disc centred (in generic terms) at location $\boldsymbol{x}$ with radius $R$ by $D(\boldsymbol{x},\ R)$, then at the moment of first detection the set of locations within which the individual must be located from perspective $A$ (the container $C_A$) is given by

$$C_{A,\,t=1} = D\left(\boldsymbol{r}^k_{t_{acc}=1},\ \gamma\right) - U, \tag{1}$$

where $\boldsymbol{r}$ is a matrix of receiver coordinates, $\boldsymbol{r}^k_{t_{acc}=1}$ denotes the location of the receiver ($k$) that detected the individual at $t_{acc} = 1$ and $\gamma$ is a constant. From perspective $B$, at $t = 1$ the set of possible locations spans a wider area, in line with the time between detections and the individual's mobility, according to the equation:

$$C_{B,\,t=1} = D\left(\boldsymbol{r}^l_{t_{acc}=2},\ \gamma + \Delta\left(t_{acc}=1,\ t_{acc}=2\right)\right) - U, \tag{2}$$

where $\Delta\left(T_1,\ T_2\right)$ is a function that defines the maximum distance the individual could move in the time between any two time indices (generically labelled $T_1$ and $T_2$). This function is defined as:

$$\Delta\left(T_1,\ T_2\right) = mobility \times \left(\tau\left(T_2\right) - \tau\left(T_1\right)\right), \tag{3}$$

where *mobility* is the maximum movement speed and $\tau(T)$ is a function that returns the 'clock' time at time index $T$. The intersection of $C_A$ and $C_B$ ($C_I$) defines the set of possible locations at $t = 1$:

$$C_{I,\,t=1} = C_{A,\,t=1} \cap C_{B,\,t=1}. \tag{4}$$

Within $C_I$, the probability of the individual being in any given location according to the AC algorithm, $\Pr\left(\boldsymbol{s}^i \mid AC\right)$, may vary given variation in detection probability (Figure S1). A standard detection probability model is a logistic model where the probability of a detection event at receiver $k$ at time $t$ ($ev\left[k,\ t\right]$), given a transmission from $\boldsymbol{s}^i$, declines with the Euclidean distance ($\|\cdot\|$) between the two locations:

$$\Pr\left(ev\left[k,\ t\right] \mid \boldsymbol{s}^i\right) \sim logistic\left(\alpha - \beta \times \left|\boldsymbol{s}^i - \boldsymbol{r}^k\right|\right) = \frac{1}{1 + e^{-\left(\alpha - \beta \times \left|\boldsymbol{s}^i - \boldsymbol{r}^k\right|\right)}}, \tag{5}$$

where $\alpha$ and $\beta$ are parameters. In a simple array, this model implies that the probability of the individual being in location $\boldsymbol{s}^i$ given a detection at $k$ declines with distance in the same way:

$$\Pr\left(\boldsymbol{s}^i \mid ev\left[k,\ t\right]\right) \sim logistic\left(\alpha - \beta \times \left|\boldsymbol{s}^i - \boldsymbol{r}^k\right|\right), \tag{6}$$

where $\sum_i \Pr(\boldsymbol{s}^i \mid \text{ev}[k,\ t]) = 1$ (see Supporting Information S1.1).

Moving forwards in time, we can consider a sequence of intermediate time steps before the next detection (Figure S1). During this time, from the perspective of the individual's previous location ($A$), the set of possible locations of the individual expands (in line with *mobility*) because it could have moved beyond its previous location. At time step $t+1$ the container $C_{A,t+1}$ will contain all locations ($\boldsymbol{z}$) at most a distance of $\Delta(t,\ t+1)$ beyond the previous container $C_{l,t}$:

$$C_{A,t+1} = \left\{ \boldsymbol{z}^i \text{ such that } \left|\boldsymbol{z}^i - \boldsymbol{p}\right| \le \Delta(t,\ t+1) \text{ for any } \boldsymbol{p} \in C_{l,t} \right\} - U, \quad (7)$$

where $\boldsymbol{p}$ represents all locations in $C_{l,t}$. Meanwhile, from perspective $B$, the set of possible locations shrinks, as the individual must have been located within the detection container of that receiver by the time of the next detection:

$$C_{B,t+1} = D\left(\boldsymbol{r}^l_{t_{acc}=2},\ \gamma + \Delta\left(t+1,\ t_{acc}=2\right)\right) - U. \quad (8)$$

At each time step, the intersection of the containers defines the set of possible locations of the individual:

$$C_{l,t+1} = C_{A,t+1} \cap C_{B,t+1}. \quad (9)$$

During this time, the probability of the individual being at location $\boldsymbol{s}^i$ in $C_l$, given the absence of a detection at $k$ ($ev^c[k,\ t]$), increases with distance from receivers:

$$\Pr\left(\boldsymbol{s}^i \mid ev^c[k,\ t]\right) \sim 1 - logistic\left(\alpha - \beta \times \left|\boldsymbol{s}^i - \boldsymbol{r}^k\right|\right), \quad (10)$$

where $\sum_i \Pr(\boldsymbol{s}^i \mid ev^c[k,\ t]) = 1$ (see Supporting Information S1.1).

Collectively, these dynamics recognise that as time passes between detections the individual could have moved away from the receiver that recorded the previous detection but only at a rate and in a direction that fits with the receiver that recorded the next detection. Thus, when the individual is detected again, the set of possible locations collapses to the detection container around the relevant receiver (and its intersection with previous and future containers) (Figure S1).

The result is a set of surfaces that describe the individual's possible locations though time. Their sum (over the number of time steps) defines a utilisation distribution that describes the expected proportion of time steps spent in each location—a metric termed 'proportion-of-use' (POU). The key innovation of this framework is the mechanistic perspective that exploits information both within and between detections, through the incorporation of detection probability, movement barriers and mobility and the flexibility with which it can incorporate additional information (see S2.3–5).

## 2.3 | Depth-contour algorithm

The DC algorithm captures the information provided by depth observations (Figure S2). In general terms, this algorithm represents the probability of a tagged animal being in a location ($\boldsymbol{s}^i$) at time $t$ according to a depth-error model ($f$) that depends on the bathymetric depth in that location ($bathy(\boldsymbol{s}^i_t)$) and the observed depth ($depth_t$):

$$\Pr\left(\boldsymbol{s}^i \mid depth_t\right) = f\left(bathy(\boldsymbol{s}^i_t),\ depth_t\right). \quad (11)$$

For example, we could consider all locations in which the bathymetric depth is deeper than a lower limit and shallower than an upper limit, given two depth-error functions ($\varepsilon_{lower}$ and $\varepsilon_{upper}$), as possible locations of the individual with uniform probability:

$$\Pr\left(\boldsymbol{s}^i \mid DC\right) = \Pr\left(\boldsymbol{s}^i \mid depth_t\right) \sim \begin{cases} a & \text{if } depth_t + \varepsilon_{lower}(depth_t) \le bathy(\boldsymbol{s}^i_t) \le depth_t + \varepsilon_{upper}(depth_t) \\ 0 & \text{otherwise} \end{cases}, \quad (12)$$

where $a$ is a positive constant that defines possible locations of the individual, chosen such that $\sum_i \Pr(\boldsymbol{s}^i \mid DC) = 1$. This model is suitable for both benthic and pelagic species and permits depth-dependent measurement errors. As for the AC algorithm, the result is a set of surfaces that describe the expected proportion of time steps spent in each $\boldsymbol{s}^i$ (POU) and the extent to which an area captures an animal's depth preferences (i.e. habitat representation). It also provides a means to incorporate depth within the AC algorithm (see S2.4).

## 2.4 | Acoustic-container depth-contour algorithm

The ACDC algorithm integrates the AC and DC algorithms (Figure S3). At each time step, the AC algorithm defines the containers of the individual's possible location and within these the DC algorithm isolates the grid cells that meet depth constraints. At each step, the probability of each location is the (normalised) product of the probabilities derived from each algorithm:

$$\Pr\left(\boldsymbol{s}^i \mid ACDC\right) \sim \Pr\left(\boldsymbol{s}^i \mid AC\right) \times \Pr\left(\boldsymbol{s}^i \mid DC\right). \quad (13)$$

## 2.5 | Particle filtering algorithms

AC-branch algorithms can be extended via a PF process that incorporates a movement model to refine the set of possible locations of a tagged individual through time (Figure S4). Coupled with the AC, DC and ACDC algorithms, the combined workflow forms the ACPF, DCPF and ACDCPF algorithms (Table 1).

PF proceeds as follows. At the first time step, $q$ locations ('particles') are sampled (with replacement) from the set of possible locations, according to probabilities from an AC-branch algorithm; that is, $\Pr\left(\boldsymbol{s}^i_{t=1} \mid \psi\right)$ where $\psi \in \{AC,\ DC,\ ACDC\}$. For each particle, movement probabilities to surrounding locations are assigned from a predefined movement model. In general, movement probabilities may depend on properties of the route between two locations ($\boldsymbol{s}^i_t$ and $\boldsymbol{s}^i_{t+1}$) and temporal variables ($b$):

$$\Pr\left(\boldsymbol{s}^i_{t+1} \mid \boldsymbol{s}^i_t\right) = g\left(\boldsymbol{s}^i_t,\ \boldsymbol{s}^i_{t+1};\ b_t\right), \quad (14)$$

where $g$ is some function. For example, we could consider a model in which movement probabilities decline logistically with Euclidean or shortest distances between locations, with the rate of decline dependent on predefined behavioural states ($b \in \{0, 1\}$), such as:

$$\Pr\left(\boldsymbol{s}_{t+1}^{i} \mid \boldsymbol{s}_{t}^{i}\right) = \begin{cases} logistic\left(\alpha_1 - \beta_1 \times h\left(\boldsymbol{s}^{i}, \boldsymbol{s}^{j}\right)\right) & \text{if } b = 0 \\ logistic\left(\alpha_2 - \beta_2 \times h\left(\boldsymbol{s}^{i}, \boldsymbol{s}^{j}\right)\right) & \text{otherwise} \end{cases} \quad (15)$$

where $h\left(\boldsymbol{s}^{i}, \boldsymbol{s}^{j}\right)$ is a measure of the distance between $\boldsymbol{s}^{i}$ and $\boldsymbol{s}^{j}$. For each particle, location probabilities from an AC-branch algorithm for the next time step are updated with these movement probabilities:

$$\Pr\left(\boldsymbol{s}_{t+1}^{i} \mid \psi, \boldsymbol{s}_{t}^{i}\right) \sim \Pr\left(\boldsymbol{s}_{t+1}^{i} \mid \psi\right) \times \Pr\left(\boldsymbol{s}_{t+1}^{i} \mid \boldsymbol{s}_{t}^{i}\right). \quad (16)$$

At subsequent time steps, this process repeats, with $q$ new locations ('particles') sampled according to their probability, given the set of possible locations and previously sampled particles. The result is a time series of particle samples that are consistent with the data and model parameters.

## 2.6 | From particles to maps and paths

Particles can be used to build maps of space use and reconstruct movement paths (Figure S5). For mapping, we suggest the POU metric, derived from particle samples, alongside smoothing techniques (see Supporting Information S1.2–4). For path reconstruction, we define an algorithm that links particles into movement paths (see Supporting Information S1.4).

## 2.7 | Simulation

We illustrate, evaluate and apply the flapper algorithms using simulated and real-world data in R (R Core Team, 2022) via the flapper package (see Supporting Information S2–5; Figure S6; Table S1). To illustrate the algorithms and to evaluate their utility and sensitivity in different settings, we begin by simulation (see Supporting Information S3). We consider a $4 \times 4\,km^2$ area and 12 simulated array designs (see Supporting Information S3.1.1; Table S2). We simulate movements of a benthic animal from a discrete-time, random-walk model, with the individual taking a 'step' up to 500 m in length every 2 min, over 500 time steps (see Supporting Information S3.1.2). At each step, we imagine that the individual transmits an acoustic signal and simulate detections at receivers given a logistic detection probability model in which detection probability declines to zero by 300 m from receivers (see Supporting Information S3.1.3). Using open-access bathymetry data, we also simulate an 'observed' depth at each step from a depth-error model (see Supporting Information S3.1.4). The result is a set of detection and depth 'observations' for each array. Using these data, we implement three simulation analyses (named S1–S3 in Table S1).

For illustration purposes, we first consider one of the simulated arrays and the associated observations (S1). Starting with the AC branch, we apply the DC algorithm to the simulated depths to demonstrate its utility for examining habitat representation, using the bathymetry data and depth-error model used to simulate the data (see Supporting Information S3.2). We then apply the AC and ACDC algorithms to the detection and depth datasets in the same way to examine the extent of possible movements (see Supporting Information S3.2). Using the outputs of the AC-branch algorithms and the movement model used to simulate the data, we apply PF. We use the DCPF algorithm to reconstruct possible 'post-release' movements over the first 30 time steps and the ACPF and ACDCPF algorithms to reconstruct patterns of space use across the whole time series (see Supporting Information S3.2).

Following illustration, we evaluate algorithm utility (S2) for reconstructing patterns of space use (see Supporting Information S3.3) and sensitivity (S3) to misspecification in each array (see Supporting Information S3.4; Figure S7; Table S3). For these analyses, we visually compare POU and KUD maps of the simulated data versus those reconstructed by the mean-position algorithm (a useful reference) and the ACPF and ACDCPF algorithms.

## 2.8 | Case study

We demonstrate real-world applications using detection and depth data from flapper skate (see Supporting Information S4; Figures S8–S11; Table S1). For these analyses, the 'study area' is located within a Scottish Marine Protected Area (MPA) (see Supporting Information S4.1.1; Figure S8). We implement four analyses to investigate habitat representation (A1), reconstruct patterns of space use (A2), examine post-release movements (A3) and explore fine-scale spatial partitioning (A4). For the analyses that incorporate depth (A1–A4), we assume a depth-error model that accounts for tag error, tidal range, bathymetry error and limited movements off the seabed (see Supporting Information S4.1.2; Figure S12). For the analyses incorporating detections (A2 and A4), we assume a logistic detection probability model, with detection probability declining to zero by 750 m from receivers (see Supporting Information S4.1.3; Figure S12). For the analyses incorporating movement (A2–A4), we assume a mobility of 500 m in 2 min, with movement probabilities declining dramatically beyond 250 m following a logistic model, especially during periods of minimal vertical activity that may reflect resting behaviour (see Supporting Information S4.1.4; Figure S12). For analyses based on PF (A2–A4), we sample 1000 particles at each time step. We use Euclidean distances to sample particles but shortest distances to process particles/paths (see Supporting Information S4.2–4.4).

For analyses A1–A2, we consider the movements of a selected individual (540) over a 1-month period for which frequent detections and regular (2 min) depth observations are available (Figure S9) (Lavender et al., 2021a). In analysis A1, we apply the DC algorithm to depth observations to examine the extent to which exploited depths are represented within the study area (see Supporting

Information S4.2). In analysis A2, we use the mean-position, ACPF and ACDCPF algorithms to reconstruct patterns of space use, quantify residency and investigate sediment preferences (see Supporting Information S4.2). In analysis A3, we apply the DCPF algorithm to reconstruct the movements of two individuals (1507 and 1558) suggested to exhibit irregular post-release behaviour (IPRB), in the form of rapid re-ascents towards the surface, following catch-and-release angling (see Supporting Information S4.3; Figure S10). In analysis A4, we apply the ACDCPF algorithm to reconstruct the movements of two other individuals (542 and 560) during a period of cooccurring detections to examine fine-scale spatial partitioning (see Supporting Information S4.4; Figure S11).

The use of field data was reviewed and approved by the Ethics Committee of the University of St Andrews (number SEC21024). Data collection that involved live animals was carried out in compliance with The Animals (Scientific Procedures) Act 1986 under the Home Office Project License number 60/4411 by competent Personal License holders.

## 3 | RESULTS

### 3.1 | Simulations

Flapper algorithms can be applied to examine habitat representation, reconstruct movement paths and map space use (Figure 1; Table S4). In the simulated data analysed for illustrative purposes (Figure 1a,b), the DC algorithm indicates the extent to which

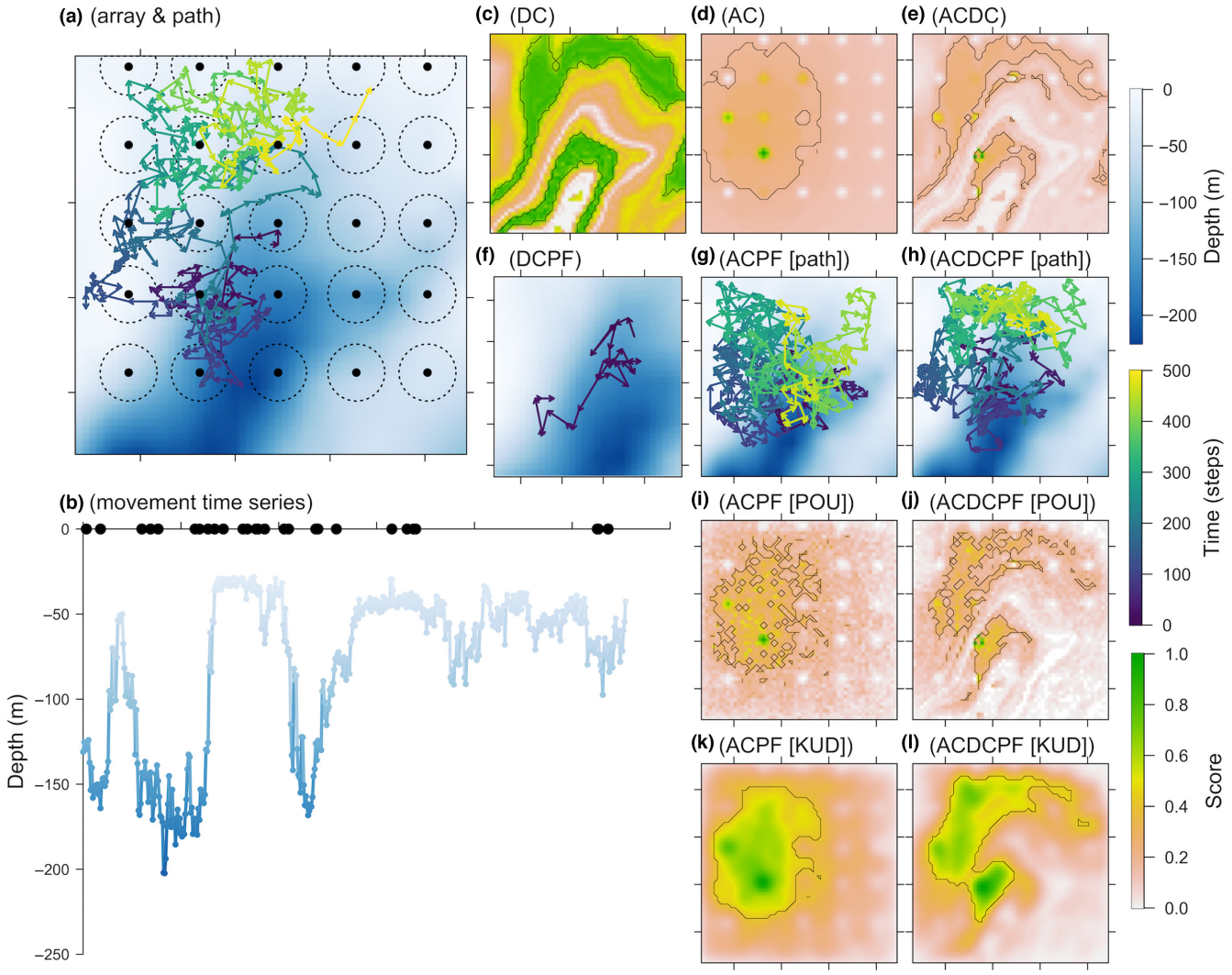


FIGURE 1 Illustrations of the flapper algorithms. (a) and (b) show simulated data for which algorithms are illustrated. (a) shows the simulated array, including the bathymetry (blue), receivers (points), detection containers (dotted circles) and a movement path (arrows). (b) shows detections (black) and depths (blue) arising from the simulated path. (c)–(l) show the results from flapper algorithms applied to these 'observations'. (c)–(e) show DC, AC and ACDC POU scores. (f)–(h) exemplify reconstructed movement paths from the DCPF, ACPF and ACDCPF algorithms. The shorter path in (f) corresponds with the shorter time interval over which the DCPF algorithm was implemented and is shown on a zoomed-in bathymetry surface. (i)–(l) exemplify the use of particles to reconstruct maps of space use in terms of POU (i, j) and KUDs (k, l). Scores are scaled by the maximum value across all panels for comparison. Lines mark 50% contours.

exploited depths are represented in the study area, highlighting shallow (~50 m) and deep (~150 m) areas that coincided with exploited depths most frequently (Figure 1c). The AC algorithm highlights peaks in POU around specific receivers (in line with the concentrating effect of detections on location probabilities) but also suggests a core range alongside the possibility of wider movements in detection gaps (Figure 1d). In the ACDC algorithm, the combination of detections with depth observations highlights a narrower region within which movements must have concentrated (Figure 1e).

PF-branch algorithms develop the AC-branch algorithms to reconstruct possible movement paths and refine maps of space use (Figure 1f–l). The DCPF algorithm reconstructs multiple 'post-release' paths (Figure 1f). Over the whole time series, the ACPF and ACDCPF algorithms reveal further paths consistent with the data (Figure 1g,h). Early in the time series, when detections were most frequent, illustrated and simulated paths overlap most heavily. This is especially true for the ACDCPF-derived path, for which initial particle samples were restricted to the deep-water area within which the individual was initially located. However, the reconstructed paths spread out over time, in line with the limited geographic restrictions on the individual's possible locations in detection gaps in a relatively homogenous bathymetric landscape.

Beyond movement paths, particle samples from the ACPF and ACDCPF algorithms reveal emergent patterns of space use (Figure 1i–l). POU maps are detailed but pixelated (Figure 1i,j) while KUDs smooth pixel-level variation to illustrate broad patterns (Figure 1k,l). For the ACPF algorithm, POU concentrates at specific receivers but wider patterns broadly correspond with the simulated path, though movements beyond the boundaries of the simulated path allowed by the 'observations' mean that reconstructed patterns are broader than those for the simulated path. For the ACDCPF algorithm, reconstructed patterns also encapsulate the simulated path but depart from the shape of simulated patterns as a result of the influence of the depth 'observations' and the shape of the bathymetry: while the simulated individual mainly exploited shallow-water habitats in the west, the 'observations' are also consistent with the exploitation of areas further east where these depth contours trace the edges of the central basin.

Across simulated arrays, the utility of the ACPF and ACDCPF algorithms for reconstructing patterns of space use varies but often compares favourably with the mean-position algorithm (Figure 2; Figures S13–S15; Table S5). For all algorithms, performance is higher in arrays with more and regularly arranged receivers. Qualitatively, for the array with 25 regularly arranged receivers, the mean-position algorithm reconstructs the shape of the true pattern of space use with relatively high fidelity (Figure 2). The ACPF algorithm suggests a similar—but more diffuse—pattern, indicating potential movements to more distant locations. The ACDCPF algorithm represents the true pattern most effectively, but also highlights areas that could have been—but were not—exploited. For random or clustered arrays with similar numbers of receivers, performance is poorer. In these circumstances, the mean-position algorithm tends to generate few COA estimates that concentrate around receivers and do not capture the extent of simulated movements or the pattern of space use. For the ACPF and ACDCPF algorithms, detections at receivers similarly concentrate location probabilities, but the incorporation of movement in the gaps between detections results in less concentrated patterns that more effectively capture the extent of simulated movements. Of these two algorithms, the ACDCPF algorithm generally suggests more precise maps that better represent the simulated patterns, but also appears to highlight locations that were not—but could have been—exploited.

Patterns of space use are sensitive to parameter specification (Figures S16–S19). In our simulations, severe parameter under-estimation frequently prevented algorithm convergence, particularly in situations with stronger constraints on individual location. For example, halving the maximum detection range ($\gamma$) prevented convergence in 6/12 simulations of the ACDCPF algorithm (Figure S17). In the simulations that converged, parameter under-estimation generally concentrated patterns, with $\gamma$-under-estimation strengthening 'hotspots' over receiver locations, in line with the concentrating effect of detections on location probability (Figures S16 and S17); and *mobility*-under-estimation strengthening 'hotpots' in-between receivers, where the simulated individual spent most time (Figures S18 and S19). In contrast, parameter over-estimation suggested wider patterns of movement, with elevated 'hotspots' in-between receivers (with elevated $\gamma$: Figures S16 and S17) and low probability movements further afield (with elevated *mobility*: Figures S18 and S19). In most cases, these discrepancies increase relatively steadily with the degree of misspecification, but appear to plateau at elevated mobilities in most simulated arrays (Figures S18 and S19).

## 3.2 | Case study

Applied to flapper skate datasets, the flapper algorithms indicate patterns of space use, possible habitat preferences and fine-scale movements (Figure 3; Figure S20). The application of the DC algorithm indicates that most of the study area could have been used over the time window examined (Figure 3a; Table S6). However, there are specific areas in which bathymetric depths overlapped more often with observed depths. They represent habitats potentially favoured on the basis of their depth (for the selected time series).

Moving beyond the DC algorithm, patterns of space use reconstructed from the mean-position, ACPF and ACDCPF algorithms differ (Figure 3b–d; Figure S20; Tables S6 and S7). The mean-position algorithm's KUD broadly corresponds with a map of detection days while the ACPF and ACDCPF algorithms suggest more diffuse patterns of space use that illustrate the extent of possible movements beyond receivers (Figure 3c,d; Figure S20). Importantly, both flapper algorithms demonstrate that the individual could have remained in

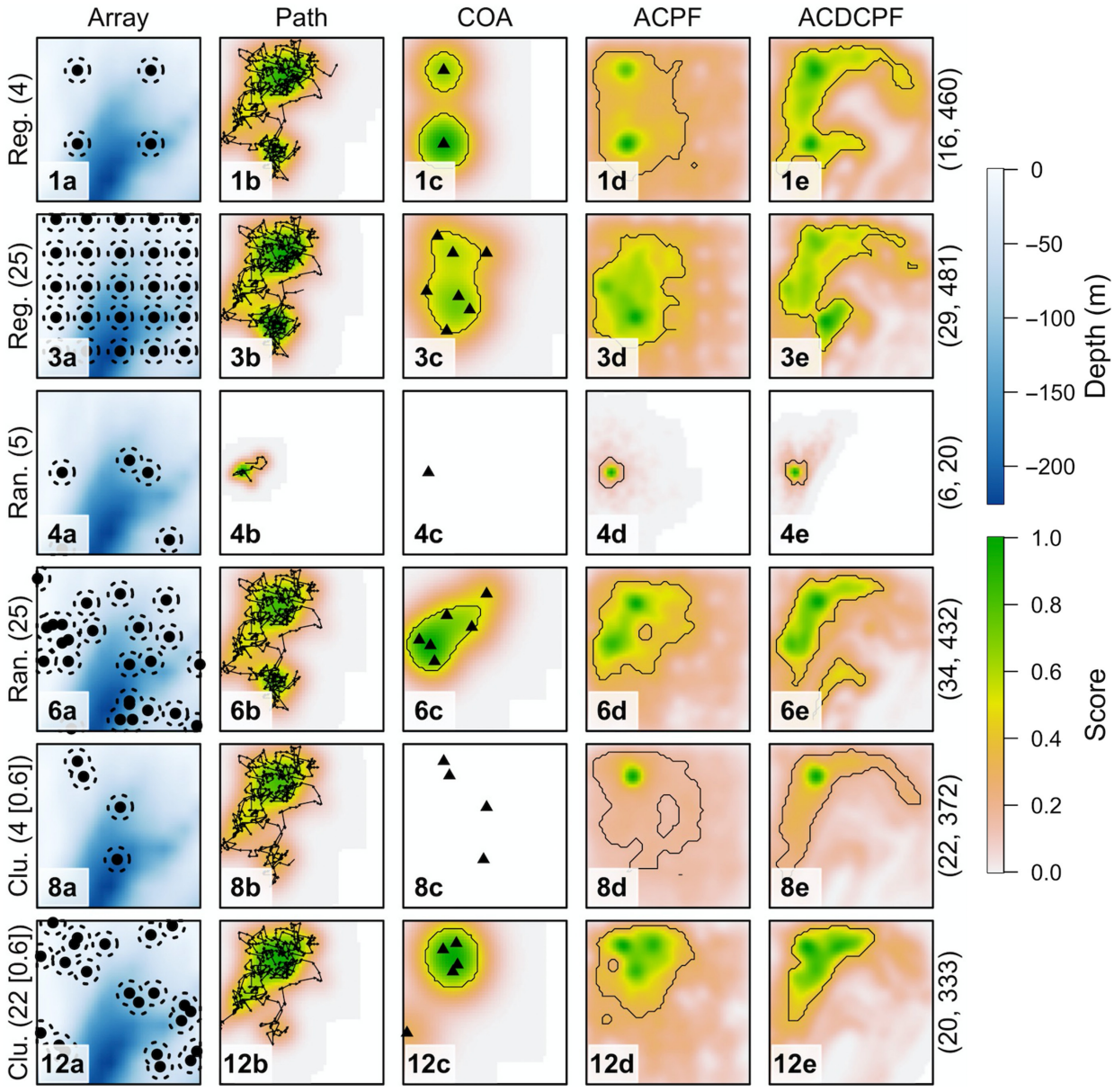


**FIGURE 2** Simulation-based evaluation of the flapper algorithms for reconstructing patterns of space use. For each row, the array (a) is shown (with bathymetry) and numbered following Table S2 alongside reconstructed patterns of space use (b–e). Illustrated arrays comprise regular, random or clustered (parameter = 0.6, if applicable) arrangements with 'few' (~5) or 'many' (~25) receivers, as denoted on the left. The number of detection and depth 'observations' per array is given in brackets on the right. For each array, the portion of the simulated path between the first and last detections (b) is shown; while the underlying path was the same for all simulations (Figure 1a), there are differences in illustrated paths due to differing detection data from each array. KUDs from COAs (triangles) (c) and the ACPF (d) and ACDCPF (e) algorithms are shown for simulations that generated sufficient 'observations'. Scores are scaled row-wise by the maximum value. Lines mark 50% contours.

**FIGURE 3** Applications of the flapper algorithms illustrating habitat representation (a), space use (b–d), habitat preferences (e) and movement paths (f–h) for selected flapper skate. (a)–(d) show reconstructed patterns of space use for an example individual (540) over a 1-month period from the DC, mean-position, ACPF and ACDCPF algorithms (analyses A1–A2). POU (a) and KUD (b–d) scores are scaled to a maximum value of one (separately in (a) and (b–d)). Lines mark core ranges (50% contours). These maps are not 'equally plausible' but show how the integration of different sources of information affects inferences; the inclusion of acoustic and archival data in the ACDCPF algorithm produces the most refined map. (e) shows the implications of reconstructed patterns of space use for an analysis of sediment preferences comparing the 'background' proportion of each sediment type available (AV) in the study area versus the core range for individual 540 inferred from each algorithm (shown in b–d). (f)–(h) show reconstructed movement paths from analyses A3–A4. (f) and (g) show the 10 most likely post-release paths off two islands (Kerrera and Insh) reconstructed by the DCPF algorithm for individuals 1507 and 1558 (A3). (h) shows the most likely paths reconstructed by the ACDCPF algorithm for two other individuals during a period of overlapping detections at one receiver (A4). For all paths (f–h), shortest paths are drawn between sequential locations. Bathymetry and coastline data were sourced from Howe et al. (2014) and Digimap. Digimap data © Crown copyright and database rights [2019] Ordnance Survey (100025252).

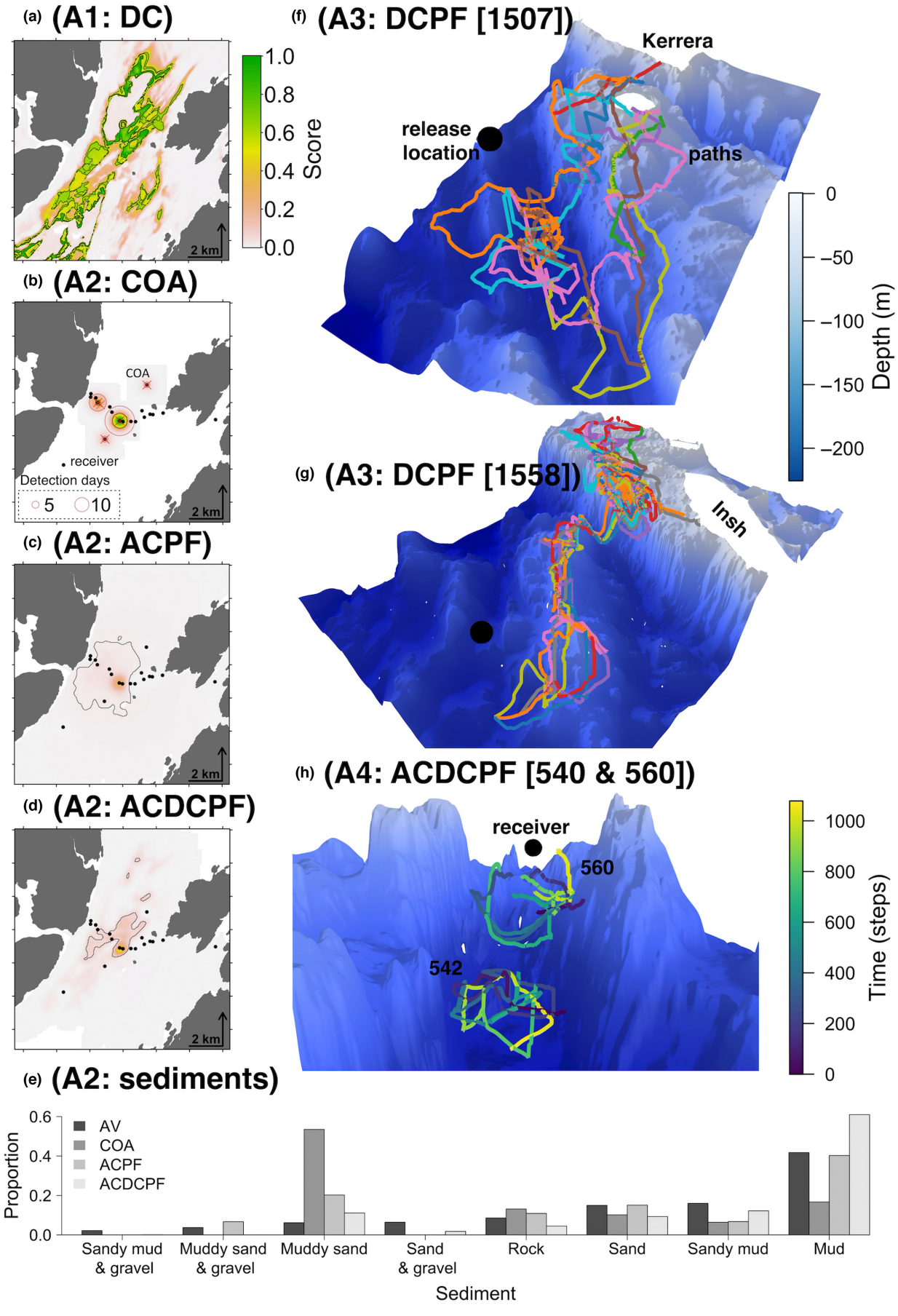

the study area throughout the study period, despite detection gaps lasting up to 43.70 h. Indeed, the ACDCPF algorithm suggests relatively restricted movements within deep-water channels during this time (Figure 3d; Figure S8). Assuming this result broadly applies to the flapper skate analysed by Lavender et al. (2021a), estimates for the minimum time that tagged individuals spent in the area increase from 1–256 (median = 34) to 2–324 (median = 42) days.

Differences in reconstructed patterns of space use have implications for home-range (Figure 3b–d) and habitat preference analyses (Figure 3e). According to the mean-position algorithm, the prevalence of muddy sand within the individual's core range exceeds background levels. However, the ACPF and ACDCPF algorithms suggest that this result is an artefact of COAs' localised distribution; accounting for possible movements beyond receivers indicates that muddy sand is only marginally more prevalent than expected.

Alongside patterns of space use, the DCPF and ACDCPF algorithm applications reveal fine-scale movements (Figure 3f–h). The application of the DCPF algorithm to two individuals that exhibited IPRB shows that the rapid post-release ascents of these individuals are consistent with benthic/demersal behaviour, despite the ascent rate (Figure 3f,g; Table S6). Meanwhile, during a period of overlapping detections for individuals 542 and 560, the application of the ACDCPF algorithm suggests fine-scale spatial partitioning (Figure 3h; Table S6).

## 4 | DISCUSSION

This study provides a holistic framework and a family of algorithms for modelling PAT data. The central development is the recapitulation of the movement and detection processes that generate observations, including detections, detection gaps and ancillary data. The algorithms provide a means to reconstruct fine-scale movements and investigate their drivers, examine emergent patterns of space use and infer habitat preferences for both benthic and pelagic species. For reconstructing patterns of space use, the methods compare favourably with the mean-position algorithm, producing maps that more effectively illustrate the distribution of possible movements (particularly in clustered arrays) and provide a means to quantify residency through detection gaps. For flapper skate, the illustrative applications extend research on movement (Lavender et al., 2021a), depth use (Thorburn et al., 2021) and disturbance responses (Lavender, Aleynik, Dodd, Illian, James, Wright, et al., 2022), revealing for the first time movements following disturbance and fine-scale spatial partitioning. For the selected individual, the results strengthen the evidence for localised movements in the MPA, supporting the view that spatial management can contribute towards skate conservation (Lavender et al., 2021a). For mobile aquatic species more broadly, there is significant potential for this line of research to support the implementation of conservation measures such as MPAs.

Our framework extends existing 'synthetic path' approaches, especially Aspillaga et al.'s (2019) simulation-based methodology. A key innovation is the separate representation of locational and movement information. This two-step framework provides a flexible means to combine datasets in the reconstruction of possible locations (the AC branch) and their linkage into movement paths (the PF branch). In the AC branch, at the moment of detection, our calculations permit any array design, including designs with overlapping receivers. At subsequent time steps, our approach can utilise information in detection gaps or consider sequential detections (as in Aspillaga et al.'s (2019) methodology). The representation of detection gaps is a significant development because it permits a fuller exploration of possible movements than permitted under the assumption that individuals follow least-cost paths between detection containers. In situations with ancillary data, this approach also facilitates modelling movement at temporal resolutions limited by ancillary data rather than detections, which are often sparser. The PF branch provides a flexible means to integrate movement probabilities into this process. During PF, our application can incorporate movement probabilities based on Euclidean or shortest distances, alongside time-specific variables, such as behaviour, informed by ancillary data. The shortest-distance routines themselves also improve upon those implemented elsewhere (Aspillaga et al., 2019; Niella et al., 2020) due to the exploitation of effective approximations and efficient C++ routines (Larmet, 2019).

The framework we advance provides opportunities to reconstruct fine-scale movements, improved maps of space use and support habitat preference analyses. For reconstructing maps of space use, simulations illustrate that the mean-position and flapper algorithms fall at opposite ends of a precision/bias spectrum. In the mean-position algorithm, COAs are estimated from receiver locations, which means that maps of space use are relatively precise but can be biased by receiver locations. The flapper algorithms are also influenced by the concentrating effect of detections on location probabilities, but the incorporation of movement reduces the influence of array design, generating more diffuse maps. In regular, high-coverage arrays, simulations suggest that both approaches can be instructive, though residency during detection gaps can only be estimated from the latter. In contrast, in clustered arrays, particle-based maps can better encapsulate the extent of movement. The distribution of possible movements may be wider and shaped differently from the true path, but it is more useful for prediction (the bias–variance trade-off). In sparse arrays, neither approach is informative.

A challenge for applications of our framework is the data required on detection probability and movement. Our simulations re-affirm the importance of these processes and we encourage systems that record detections alongside data on detection probability and movement speeds to support inference (Kessel et al., 2014). For our framework, simulations suggest a degree of robustness to the value of any one parameter that emerges from the interactions of multiple constraints. However, as for any model, misspecification may mislead inferences, suggesting overly concentrated patterns of space use (with parameter under-estimation) or overly extensive ones (with parameter over-estimation) that are shaped by array design and other constraints. Thus, further research into algorithm sensitivity in different settings is worthwhile.

Computational requirements also challenge applications of our framework. While AC-branch algorithms are deterministic, often parallelisable and relatively fast, PF is generally slower because each sample is contingent upon previous samples. Consequently, for big datasets, focusing on periods of frequent detections, thinning and/or reducing an analysis' temporal resolution may be beneficial. Given the accumulation of PAT data (Matley et al., 2022), detailed evaluation of the consequences of these choices, alongside further computational optimisation, would be beneficial.

For the case-study species, our illustrative analyses indicate responses to catch-and-release angling, fine-scale partitioning and localised movements. The post-release analyses demonstrate that the rapid ascents of two individuals suggested to exhibit IPRB are consistent with movement over the seabed, despite their irregularity. These analyses represent an important step in understanding responses to capture and how they are shaped by the environment (Lavender, Aleynik, Dodd, Illian, James, Wright, et al., 2022). For the two individuals with cooccurring detections, the analyses suggest fine-scale spatial partitioning rather than close-knit interactions. This demonstrates that multiple individuals may inhabit a similar ($<0.5\,km^2$) area at the same time while behaving differently, as previously suggested (Lavender et al., 2021a). The space-use analyses suggest that localised movements may continue over longer timescales, with continuous residency of individual 540 in a $13\times13\,km$ area over 1 month fully consistent with the data. While this result does not preclude movements further afield, it strengthens the evidence that residency in the study area may continue through detection gaps (Lavender et al., 2021a). During this time, the graphical habitat preference analysis points towards the exploitation of multiple benthic habitats, in concordance with recent work (Thorburn et al., 2021).

A limitation with our case-study analyses is the lack of information on movement speeds. While we suggest methods for inferring mobility from PAT data (in Supporting Information S4.1.4), high-resolution activity data would support expansion of our analyses. Building on recent studies, the flapper algorithms could refine population-level maps of depth representation and enable examination of fine-scale movements, population-level patterns of space use, residency and habitat preferences (Lavender et al., 2021a; Lavender, Aleynik, Dodd, Illian, James, Wright, et al., 2022; Thorburn et al., 2021). This information is critical in the design of MPAs for mobile species (MacKeracher et al., 2019).

Continued methodological research will support applications of our framework and existing approaches. Important areas of future research include computational optimisation, method sensitivity and the relative merits of existing methods in diverse contexts. Our methodology may also offer unexplored opportunities to optimise tag and array deployment programmes, through simulation-based comparisons of alternative options. Nevertheless, all approaches are limited by available data and there is no panacea to the reconstruction of movements over long detection gaps. Thus, coupled development of tagging and array deployment programmes alongside analytical approaches is crucial for continued progress.

## AUTHOR CONTRIBUTIONS

Edward Lavender conceived the ideas and designed the methodology, with inputs from all co-authors (especially Sophie Smout, Janine Illian and Stanisław Biber); James Thorburn collected the data; Edward Lavender analysed the data; Edward Lavender and Stanisław Biber led the writing of the manuscript. All authors (Edward Lavender, Stanisław Biber, Janine Illian, Mark James, Peter J. Wright, James Thorburn and Sophie Smout) contributed critically to the drafts and gave final approval for publication.

## ACKNOWLEDGEMENTS

We appreciated discussions with Jason Matthiopoulos, Richard Glennie, Carl Donovan, Andrew Seaton, David Miller, Helen Moor and Andreas Scheidegger. The work was supported by a PhD Studentship at the University of St Andrews funded by NatureScot, via the Marine Alliance for Science and Technology for Scotland (MASTS), and the Centre for Research into Ecological and Environmental Modelling. Data were made available through the Movement Ecology of Flapper Skate project funded by NatureScot (project 015960) and Marine Scotland (projects SP004 and SP02B0). Jane Dodd, Ronnie Campbell, Roger Eaton, Francis Neat and Dmitry Aleynik supported this project. MASTS and Shark Guardian provided additional funding. MASTS is funded by the Scottish Funding Council (grant reference HR09011) and contributing institutions.

## CONFLICT OF INTEREST STATEMENT

The authors declare no conflict of interest.

## PEER REVIEW

The peer review history for this article is available at https://www.webofscience.com/api/gateway/wos/peer-review/10.1111/2041-210X.14193.

## DATA AVAILABILITY STATEMENT

The flapper R package is available on GitHub (https://github.com/edwardlavender/flapper) and archived on Zenodo at https://doi.org/10.5281/zenodo.8150971 (Lavender et al., 2023a). Code for simulation analyses is available via Zenodo at https://doi.org/10.5281/zenodo.8150926 (Lavender et al., 2023b). Skate data and code for case-study analyses is available via Zenodo at https://doi.org/10.5281/zenodo.8150940 (Lavender et al., 2023c).

## ORCID

*Edward Lavender* https://orcid.org/0000-0002-8040-7489
*Stanisław Biber* https://orcid.org/0000-0001-5157-2904
*Mark James* https://orcid.org/0000-0002-7182-1725
*Peter J. Wright* https://orcid.org/0000-0002-8402-5795
*James Thorburn* https://orcid.org/0000-0002-4392-1737
*Sophie Smout* https://orcid.org/0000-0002-5125-9827

## REFERENCES

Aspillaga, E., Safi, K., Hereu, B., & Bartumeus, F. (2019). Modelling the three-dimensional space use of aquatic animals combining topography

and Eulerian telemetry data. *Methods in Ecology and Evolution*, *10*(9), 1551–1557. https://doi.org/10.1111/2041-210X.13232

Block, B. A., Teo, S. L. H., Walli, A., Boustany, A., Stokesbury, M. J. W., Farwell, C. J., Weng, K. C., Dewar, H., & Williams, T. D. (2005). Electronic tagging and population structure of Atlantic bluefin tuna. *Nature*, *434*(7037), 1121–1127. https://doi.org/10.1038/nature03463

Dodd, J., Baxter, J. M., Donnan, D. W., James, B. D., Lavender, E., McSorley, C. A., Mogg, A. O. M., & Thorburn, J. (2022). First report of an egg nursery for the Critically Endangered flapper skate *Dipturus intermedius* (Rajiformes: Rajidae). *Aquatic Conservation: Marine and Freshwater Ecosystems*, *32*(10), 1647–1659. https://doi.org/10.1002/aqc.3857

Doherty, T. S., Hays, G. C., & Driscoll, D. A. (2021). Human disturbance causes widespread disruption of animal movement. *Nature Ecology & Evolution*, *5*(4), 513–519. https://doi.org/10.1038/s41559-020-01380-1

Fudickar, A. M., Jahn, A. E., & Ketterson, E. D. (2021). Animal migration: An overview of one of nature's great spectacles. *Annual Review of Ecology, Evolution, and Systematics*, *52*, 479–497. https://doi.org/10.1146/annurev-ecolsys-012021-031035

Hays, G. C., Bailey, H., Bograd, S. J., Bowen, W. D., Campagna, C., Carmichael, R. H., Casale, P., Chiaradia, A., Costa, D. P., Cuevas, E., Nico de Bruyn, P. J., Dias, M. P., Duarte, C. M., Dunn, D. C., Dutton, P. H., Esteban, N., Friedlaender, A., Goetz, K. T., Godley, B. J., … Sequeira, A. M. M. (2019). Translating marine animal tracking data into conservation policy and management. *Trends in Ecology & Evolution*, *34*(5), 459–473. https://doi.org/10.1016/j.tree.2019.01.009

Hostetter, N. J., & Royle, J. A. (2020). Movement-assisted localization from acoustic telemetry data. *Movement Ecology*, *8*(1), 15. https://doi.org/10.1186/s40462-020-00199-6

Howe, J. A., Anderton, R., Arosio, R., Dove, D., Bradwell, T., Crump, P., Cooper, R., & Cocuccio, A. (2014). The seabed geomorphology and geological structure of the Firth of Lorn, western Scotland, UK, as revealed by multibeam echo-sounder survey. *Earth and Environmental Science Transactions of the Royal Society of Edinburgh*, *105*(4), 273–284. https://doi.org/10.1017/S1755691015000146

Hussey, N. E., Kessel, S. T., Aarestrup, K., Cooke, S. J., Cowley, P. D., Fisk, A. T., Harcourt, R. G., Holland, K. N., Iverson, S. J., Kocik, J. F., Mills Flemming, J. E., & Whoriskey, F. G. (2015). Aquatic animal telemetry: A panoramic window into the underwater world. *Science*, *348*(6240), 1255642. https://doi.org/10.1126/science.1255642

Kessel, S. T., Cooke, S. J., Heupel, M. R., Hussey, N. E., Simpfendorfer, C. A., Vagle, S., & Fisk, A. T. (2014). A review of detection range testing in aquatic passive acoustic telemetry studies. *Reviews in Fish Biology and Fisheries*, *24*(1), 199–218. https://doi.org/10.1007/s11160-013-9328-4

Larmet, V. (2019). *cppRouting: Fast implementation of Dijkstra algorithm in R*. R package version 2.0. https://github.com/vlarmet/cppRouting

Lavender, E., Aleynik, D., Dodd, J., Illian, J., James, M., Smout, S., & Thorburn, J. (2022). Benthic animal-borne sensors and citizen science combine to validate ocean modelling. *Scientific Reports*, *12*(1), 16613. https://doi.org/10.1038/s41598-022-20254-z

Lavender, E., Aleynik, D., Dodd, J., Illian, J., James, M., Wright, P. J., Smout, S., & Thorburn, J. (2021a). Movement patterns of a Critically Endangered elasmobranch (*Dipturus intermedius*) in a Marine Protected Area. *Aquatic Conservation: Marine and Freshwater Ecosystems*, *32*(2), 348–365. https://doi.org/10.1002/aqc.3753

Lavender, E., Aleynik, D., Dodd, J., Illian, J., James, M., Wright, P. J., Smout, S., & Thorburn, J. (2021b). Environmental cycles and individual variation in the vertical movements of a benthic elasmobranch. *Marine Biology*, *168*(11), 164. https://doi.org/10.1007/s00227-021-03973-1

Lavender, E., Aleynik, D., Dodd, J., Illian, J., James, M., Wright, P. J., Smout, S., & Thorburn, J. (2022). Behavioural responses of a large, benthic elasmobranch to catch-and-release angling. *Frontiers in Marine Science*, *9*, 864344. https://doi.org/10.3389/fmars.2022.864344

Lavender, E., Biber, S., Illian, J., Wright, P. J., Thorburn, J., & Smout, S. (2023a). An integrative modelling framework for passive acoustic telemetry: Flapper R package. *Zenodo*, https://doi.org/10.5281/zenodo.8150971

Lavender, E., Biber, S., Illian, J., Wright, P. J., Thorburn, J., & Smout, S. (2023b). An integrative modelling framework for passive acoustic telemetry: Code for simulation analyses. *Zenodo*, https://doi.org/10.5281/zenodo.8150926

Lavender, E., Biber, S., Illian, J., Wright, P. J., Thorburn, J., & Smout, S. (2023c). An integrative modelling framework for passive acoustic telemetry: Data and code for case-study analyses. *Zenodo*, https://doi.org/10.5281/zenodo.8150940

Lea, J. S. E., Humphries, N. E., von Brandis, R. G., Clarke, C. R., & Sims, D. W. (2016). Acoustic telemetry and network analysis reveal the space use of multiple reef predators and enhance marine protected area design. *Proceedings of the Royal Society B: Biological Sciences*, *283*(1834), 20160717. https://doi.org/10.1098/rspb.2016.0717

MacKeracher, T., Diedrich, A., & Simpfendorfer, C. A. (2019). Sharks, rays and marine protected areas: A critical evaluation of current perspectives. *Fish and Fisheries*, *20*(2), 255–267. https://doi.org/10.1111/faf.12337

Matley, J. K., Klinard, N. V., Barbosa Martins, A. P., Aarestrup, K., Aspillaga, E., Cooke, S. J., Cowley, P. D., Heupel, M. R., Lowe, C. G., Lowerre-Barbieri, S. K., Mitamura, H., Moore, J.-S., Simpfendorfer, C. A., Stokesbury, M. J. W., Taylor, M. D., Thorstad, E. B., Vandergoot, C. S., & Fisk, A. T. (2022). Global trends in aquatic animal tracking with acoustic telemetry. *Trends in Ecology & Evolution*, *37*(1), 79–94. https://doi.org/10.1016/j.tree.2021.09.001

Mercker, M., Schwemmer, P., Peschko, V., Enners, L., & Garthe, S. (2021). Analysis of local habitat selection and large-scale attraction/avoidance based on animal tracking data: Is there a single best method? *Movement Ecology*, *9*(1), 20. https://doi.org/10.1186/s40462-021-00260-y

Nathan, R., Monk, C. T., Arlinghaus, R., Adam, T., Alós, J., Assaf, M., Baktoft, H., Beardsworth, C. E., Bertram, M. G., Bijleveld, A. I., Brodin, T., Brooks, J. L., Campos-Candela, A., Cooke, S. J., Gjelland, K. Ø., Gupte, P. R., Harel, R., Hellström, G., Jeltsch, F., … Jarić, I. (2022). Big-data approaches lead to an increased understanding of the ecology of animal movement. *Science*, *375*(6582), eabg1780. https://doi.org/10.1126/science.abg1780

Niella, Y., Flávio, H., Smoothey, A. F., Aarestrup, K., Taylor, M. D., Peddemors, V. M., & Harcourt, R. (2020). Refined Shortest Paths (RSP): Incorporation of topography in space use estimation from node-based telemetry data. *Methods in Ecology and Evolution*, *11*(12), 1733–1742. https://doi.org/10.1111/2041-210X.13484

Orrell, D. L., & Hussey, N. E. (2022). Using the VEMCO Positioning System (VPS) to explore fine-scale movements of aquatic species: Applications, analytical approaches and future directions. *Marine Ecology Progress Series*, *687*, 195–216. https://doi.org/10.3354/meps14003

Pecl, G. T., Araújo, M. B., Bell, J. D., Blanchard, J., Bonebrake, T. C., Chen, I., Clark, T. D., Colwell, R. K., Danielsen, F., Evengård, B., Falconi, L., Ferrier, S., Frusher, S., Garcia, R. A., Griffis, R. B., Hobday, A. J., Janion-scheepers, C., Jarzyna, M. A., Jennings, S., … Tuanmu, M. (2017). Biodiversity redistribution under climate change: Impacts on ecosystems and human well-being. *Science*, *355*(6332), eaai9214. https://doi.org/10.1126/science.aai9214

Pedersen, M. W., Righton, D., Thygesen, U. H., Andersen, K. H., & Madsen, H. (2008). Geolocation of North Sea cod (*Gadus morhua*) using hidden Markov models and behavioural switching. *Canadian Journal of Fisheries and Aquatic Sciences*, *65*(11), 2367–2377. https://doi.org/10.1139/F08-144

Pedersen, M. W., & Weng, K. C. (2013). Estimating individual animal movement from observation networks. *Methods in Ecology and Evolution*, *4*(10), 920–929. https://doi.org/10.1111/2041-210X.12086

R Core Team. (2022). *R: a language and environment for statistical computing* (4.2.2). R Foundation for Statistical Computing. https://r-project.org

Riotte-Lambert, L., & Matthiopoulos, J. (2020). Environmental predictability as a cause and consequence of animal movement. *Trends in Ecology & Evolution*, *35*(2), 163–174. https://doi.org/10.1016/j.tree.2019.09.009

Simpfendorfer, C. A., Heupel, M. R., & Hueter, R. E. (2002). Estimation of short-term centers of activity from an array of omnidirectional hydrophones and its use in studying animal movements. *Canadian Journal of Fisheries and Aquatic Sciences*, *59*(1), 23–32. https://doi.org/10.1139/f01-191

Sims, D. W., Southall, E. J., Humphries, N. E., Hays, G. C., Bradshaw, C. J. A., Pitchford, J. W., James, A., Ahmed, M. Z., Brierley, A. S., Hindell, M. A., Morritt, D., Musyl, M. K., Righton, D., Shepard, E. L. C., Wearmouth, V. J., Wilson, R. P., Witt, M. J., & Metcalfe, J. D. (2008). Scaling laws of marine predator search behaviour. *Nature*, *451*(7182), 1098–1102. https://doi.org/10.1038/nature06518

Thorburn, J., Wright, P. J., Lavender, E., Dodd, J., Neat, F., Martin, J. C. A., Lynam, C., & James, M. (2021). Seasonal and ontogenetic variation in depth use by a Critically Endangered benthic elasmobranch and its implications for spatial management. *Frontiers in Marine Science*, *8*, 656368. https://doi.org/10.3389/fmars.2021.656368

Udyawer, V., Dwyer, R. G., Hoenner, X., Babcock, R. C., Brodie, S., Campbell, H. A., Harcourt, R. G., Huveneers, C., Jaine, F. R. A., Simpfendorfer, C. A., Taylor, M. D., & Heupel, M. R. (2018). A standardised framework for analysing animal detections from automated tracking arrays. *Animal Biotelemetry*, *6*(1), 17. https://doi.org/10.1186/s40317-018-0162-2

Winton, M. V., Kneebone, J., Zemeckis, D. R., & Fay, G. (2018). A spatial point process model to estimate individual centres of activity from passive acoustic telemetry data. *Methods in Ecology and Evolution*, *9*(11), 2262–2272. https://doi.org/10.1111/2041-210X.13080

## SUPPORTING INFORMATION

Additional supporting information can be found online in the Supporting Information section at the end of this article.

**Figure S1:** The acoustic-container (AC) algorithm.

**Figure S2:** The depth-contour (DC) algorithm.

**Figure S3:** The acoustic-container depth-contour (ACDC) algorithm.

**Figure S4:** The particle filtering (PF) routine.

**Figure S5:** From particles to maps of space use and movement paths.

**Figure S6:** A schematic of the flapper algorithms as implemented by the flapper R package (version 0.1.0).

**Figure S7:** Logistic models for (A) detection probability and (B) movement used in simulations.

**Figure S8:** The case-study area.

**Figure S9:** Case-study acoustic and archival time series from a selected individual (540) used to reconstruct patterns of space use via the DC, mean-position, ACPF and ACDCPF algorithms (analyses A1–A2).

**Figure S10:** Case-study depth time series used to reconstruct post-release movement paths (analysis A3).

**Figure S11:** Example cooccurring acoustic and archival time series for a pair of individuals (542 and 560: analysis A4).

**Figure S12:** Models for (A) detection probability, (B) movement and (C) depth used in case-study analyses.

**Figure S13:** Evaluation of the flapper algorithms for all simulated array designs according to KUDs (simulation S2).

**Figure S14:** Evaluation of the flapper algorithms for all simulated array designs according to a second KUD estimator (simulation S2).

**Figure S15:** Evaluation of the flapper algorithms for all simulated array designs according to POU maps (simulation S2).

**Figure S16:** Sensitivity of the ACPF algorithm to the detection probability model (simulation S3).

**Figure S17:** Sensitivity of the ACDCPF algorithm to the detection probability model (simulation S3).

**Figure S18:** Sensitivity of the ACPF algorithm to the movement model (simulation S3).

**Figure S19:** Sensitivity of the ACDCPF algorithm to the movement model (simulation S3).

**Figure S20:** POU maps from the (A) ACPF and (B) ACDCPF algorithms for the selected individual (540) over a one-month period (analysis A2).

**Table S1:** An overview of simulations and case-study analyses.

**Table S2:** A summary of simulated array designs.

**Table S3:** A summary of algorithm parameter values for each simulation.

**Table S4:** Example applications and challenges for flapper algorithms.

**Table S5:** Wall times for simulations.

**Table S6:** Wall times for case-study analyses.

**Table S7:** Wall times for particle mapping in case-study analysis A2.

**Appendix S1:** Supporting figures, tables and information.

**How to cite this article:** Lavender, E., Biber, S., Illian, J., James, M., Wright, P. J., Thorburn, J., & Smout, S. (2023). An integrative modelling framework for passive acoustic telemetry. *Methods in Ecology and Evolution*, *00*, 1–13. https://doi.org/10.1111/2041-210X.14193